Nanoscale Horizons

Enhanced Upconversion and Photoconductive Nanocomposites of Lanthanide-Doped Nanoparticles Functionalized with Low-Vibrational-Energy Inorganic Ligands

Journal:	*Nanoscale Horizons*
Manuscript ID	NH-COM-10-2024-000555.R1
Article Type:	Communication
Date Submitted by the Author:	20-Dec-2024
Complete List of Authors:	Pan, Jia-Ahn; Scripps College, Department of Natural Sciences; Pitzer College, Department of Natural Sciences Qi, Xiao; Lawrence Berkeley National Laboratory, The Molecular Foundry Chan, Emory; Lawrence Berkeley National Laboratory, The Molecular Foundry

We introduce low-vibrational-energy inorganic ligands that enhance the luminescence of lanthanide-doped upconverting nanoparticles (UCNPs) and enable their integration into electronic devices. Existing ligand approaches typically employ UCNPs that are either (1) capped with organic/polymer ligands that have high vibrational energies or (2) ligand-free, leaving no protective barrier between the UCNP and the environment. Our method utilizes metal sulfide ions to charge-stabilize UCNPs and create a favorable environment that minimizes non-radiative quenching. Additionally, these inorganic ligand-capped UCNPs can be annealed to form a UCNP-semiconductor nanocomposite in which UCNPs are embedded within a non-epitaxial matrix, facilitating interfacing with other electronic components. To validate this approach, we incorporate the UCNP-semiconductor composite as the active layer in a photodetector capable of detecting UV and near-IR light. This inorganic ligand-to-matrix approach complements epitaxial shell growth, which is electrically insulating and often requires stringent growth conditions. Our findings demonstrate a new ligand-based strategy for enhancing the optical performance of UCNPs and expanding their applicability in optoelectronics.

Enhanced Upconversion and Photoconductive Nanocomposites of Lanthanide-Doped Nanoparticles Functionalized with Low-Vibrational-Energy Inorganic Ligands

Jia-Ahn Pan[1,2,3,*], Xiao Qi[2], and Emory M. Chan[2,*]

[1] *Department of Natural Sciences, Pitzer and Scripps Colleges, Claremont, California, 91711, United States*

[2] *Molecular Foundry, Lawrence Berkeley National Laboratory, Berkeley, California 94720, United States*

[3] *Chemical Sciences Division, Lawrence Berkeley National Laboratory, Berkeley, California 94720, United States*

[*]Email: jpan@natsci.claremont.edu, emchan@lbl.gov

Abstract

Upconverting nanoparticles (UCNPs) convert near-infrared (IR) light into higher-energy visible light, allowing them to be used in applications such as biological imaging, nano-thermometry, and photodetection. It is well known that the upconversion luminescent efficiency of UCNPs can be enhanced by using a host material with low phonon energies, but the use of low-vibrational-energy inorganic ligands and non-epitaxial shells has been relatively underexplored. Here, we investigate the functionalization of lanthanide-doped $NaYF_4$ UCNPs with low-vibrational-energy $Sn_2S_6^{4-}$ ligands. Raman spectroscopy and elemental mapping are employed to confirm the binding of $Sn_2S_6^{4-}$ ligands to UCNPs. This binding enhances upconversion efficiencies up to a factor of 16, consistent with an increase in the luminescent lifetimes of the lanthanide ions. Annealing $Sn_2S_6^{4-}$-capped UCNPs results in the formation of a nanocomposite comprised of UCNPs embedded within an interconnected matrix of SnS_2, enabling each UCNP to be electrically accessible through the semiconducting SnS_2 matrix. This facilitates the integration of UCNPs into electronic devices, which we demonstrate through the fabrication of a UCNP-SnS_2 photodetector that detects UV and near-IR light. Our findings show the promise of using low-phonon inorganic capping agents to enhance the properties of UCNPs while assisting their integration in optoelectronic devices.

Introduction

Lanthanide-doped upconverting nanoparticles (UCNPs) are nanoscale colloidal light emitters that absorb multiple low-energy photons and emit a higher-energy photon.[1–11] This optical property, known as upconversion luminescence (UCL), is enabled by the ladder-like energy levels of lanthanide ions doped within an inorganic host matrix. With their tunable optical properties and precise nanoscale size control, UCNPs have been used for applications such as biological imaging,[4] nano-thermometry,[5] super-resolution microscopy,[6,7] lithography,[8] optical computing,[9,10] and photodetection.[11]

The most common way to achieve efficient UCL from lanthanide ions is to embed them in inorganic host matrices such as $NaYF_4$ and $K_2Pb_2Cl_5$, whose low phonon energies reduce phonon-assisted non-radiative relaxation.[12,13] UCL efficiency can be further enhanced by growing an undoped, epitaxial shell made of the same material, allowing the active lanthanide ions to be

optically and chemically isolated from their environments. However, while the chemistry for growing high-quality epitaxial shells has been optimized for some UCNP host materials (e.g., $NaYF_4$),[14] the growth of epitaxial shells for other host materials (e.g., $K_2Pb_2Cl_5$) can be more challenging and remains an active area of research. Non-epitaxial oxide shells have been grown around UCNPs, leading to increased thermal stability;[15] however, their high phonon energies typically do not enhance UCL and may even reduce it.

The ligands that coordinate the surfaces of UCNPs also play an important role in their optical properties. While UCNP ligand modification has been studied primarily to maintain colloidal stability in various solvents and environments (e.g., in cells),[16] antenna ligands have also been used to dramatically enhance the small absorption cross-sections of UCNPs.[17] Even ligands that do not absorb light can impact the photophysics of luminescent nanocrystals by introducing or suppressing non-radiative pathways.[18,19] The UCL of UCNPs has been enhanced by small organic ligands, such as picolinic acid, which can alter the electronic structure of lanthanide dopants at the nanocrystal surfaces, demonstrating the potential of ligand engineering for UCNPs.[20] Ligand engineering is preferable to inert shell growth when a small size is needed (e.g., cell imaging and nanoscale devices). However, the high-energy vibrational modes of common organic ligands can quench UCNP luminescence, especially in the absence of passivating inorganic shells.

As an alternative to organic ligands, ionically charged inorganic compounds have been explored as capping ligands for semiconducting QDs.[21] These inorganic ligands, such as metal sulfide complexes, have been used to increase the electronic coupling between QDs, enhancing their performance in devices such as transistors and photodetectors.[22] Additionally, these heavier inorganic ligands possess lower vibrational energies, which may help reduce nonradiative quenching of lanthanide excited states in UCNPs. However, it remains an open question whether the chemically-"soft" sulfide ligands—typically used to coordinate with the soft Lewis acid cations in QDs—are compatible with the hard lanthanide ions in UCNPs.

Here, we investigate the use of a tin(IV) sulfide complex ($Sn_2S_6^{4-}$) as a low-vibrational-energy inorganic ligand for $NaYF_4$ UCNPs (**Scheme 1**). We explored chemical approaches to replace the native oleate ligands with the $Sn_2S_6^{4-}$ ligands and confirmed the successful ligand exchange via Raman and energy-dispersive X-ray spectroscopy (EDS). Optically, we found that the UCL efficiencies of UCNPs were enhanced by this exchange, with the greatest enhancements

observed for small and highly doped UCNPs (showing UCL enhancements up to a factor of 16). We show that the $Sn_2S_6^{4-}$ ligands can be transformed into a SnS_2 matrix upon annealing at 350 °C, forming a UCNP-SnS_2 nanocomposite. Finally, we fabricate a proof-of-concept UV and NIR photodetector using the solution-deposited UCNP-SnS_2 nanocomposite. These findings reveal a potential pathway for using inorganic ligands to enhance the properties and applications of UCNPs.

Scheme 1. Ligand exchange of oleate-capped $NaYF_4$ UCNPs with $Sn_2S_6^{4-}$ ligands and subsequent annealing into a UCNP-SnS_2 nanocomposite.

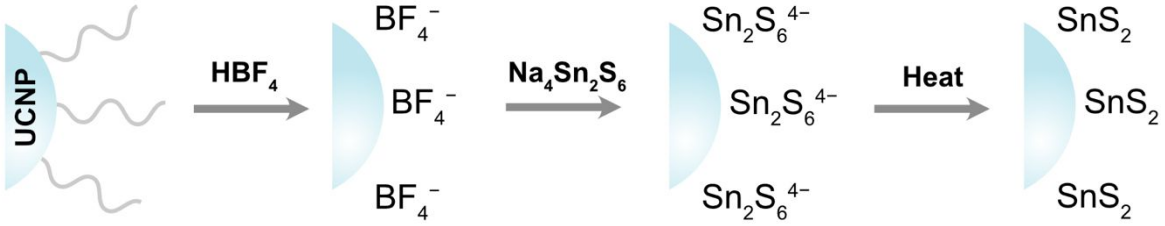

Results and Discussion

Functionalization of UCNPs with $Sn_2S_6^{4-}$ ligands

Lanthanide-doped $NaYF_4$ UCNPs and $Na_4Sn_2S_6$ ligands were synthesized according to established protocols (see Methods and Supporting Information for details).[23,24] We initially attempted ligand exchange by directly adding the $Sn_2S_6^{4-}$ ligand to a toluene dispersion of UCNPs. However, after stirring for several hours, no nanoparticle aggregation was observed, indicating that this method was ineffective in facilitating ligand exchange.

We also explored a two-phase direct exchange that involved stirring oleate-capped UCNPs in hexanes with an immiscible layer of NMF containing dissolved $Sn_2S_6^{4-}$ ligands. After stirring for 24 h, the UCNPs were observed to have either aggregated at the solvent interface or in the polar phase. Upon extraction, these UCNPs were unable to be redispersed in either a non-polar hexane solution or a polar NMF solution, implying that the ligand exchange was incomplete, i.e., UCNPs were only partially coated with $Sn_2S_6^{4-}$ ligands.

Our most successful direct exchange approach involved mixing oleate-capped UCNPs with $Sn_2S_6^{4-}$ ligands in NMF. After sonicating the suspension for a few hours, a small fraction of the UCNPs were observed to be dispersed in the NMF solution (with a larger fraction remaining

aggregated). The aggregated UCNPs were then removed by centrifugation, leaving a supernatant of colloidally dispersed, $Sn_2S_6^{4-}$-capped UCNPs.

Considering the challenges faced with direct ligand exchange, we hypothesized that $Sn_2S_6^{4-}$ functionalization could be improved by first removing the oleate ligands before functionalization. This two-step *indirect* ligand exchange process first involves stripping the oleate ligands from UCNPs using HBF_4, resulting in bare but electrically charged UCNPs that can be dispersed in a polar solvent.[8] Then, $Sn_2S_6^{4-}$ ligands are added to coat the bare UCNPs. We theorized that this indirect approach may be more effective since it circumvents the need for $Sn_2S_6^{4-}$ to directly displace strongly bound oleate ligands.

To evaluate the effectiveness of our ligand exchange procedures, we characterized the $Sn_2S_6^{4-}$-capped UCNPs with Raman spectroscopy and electron microscopy. The Raman spectra of $Sn_2S_6^{4-}$-capped $NaYF_4$ UCNPs obtained through direct and indirect ligand exchange approaches were similar, showing a distinct peak at 182 cm^{-1} as well as a cluster of peaks in the region of 250−350 cm^{-1} (**Figure 1A**, red). We attribute the 182 cm^{-1} peak to a vibrational mode of UCNP-bound $Sn_2S_6^{4-}$ ligands, which is close to the 190 cm^{-1} peak that we observe in the Raman spectrum of $Na_4Sn_2S_6$ (**Figure 1A**, grey). On the other hand, the cluster of peaks at 250−350 cm^{-1} can be primarily attributed to the phonon modes of hexagonal-phase $NaYF_4$, which were also observed in oleate-capped UCNPs (**Figure 1A**, blue).[25] We note that $Na_4Sn_2S_6$ also has a strong peak around 350 cm^{-1}, but it overlaps with the $NaYF_4$ peaks and cannot be unambiguously determined in $Sn_2S_6^{4-}$-capped $NaYF_4$ UCNPs.

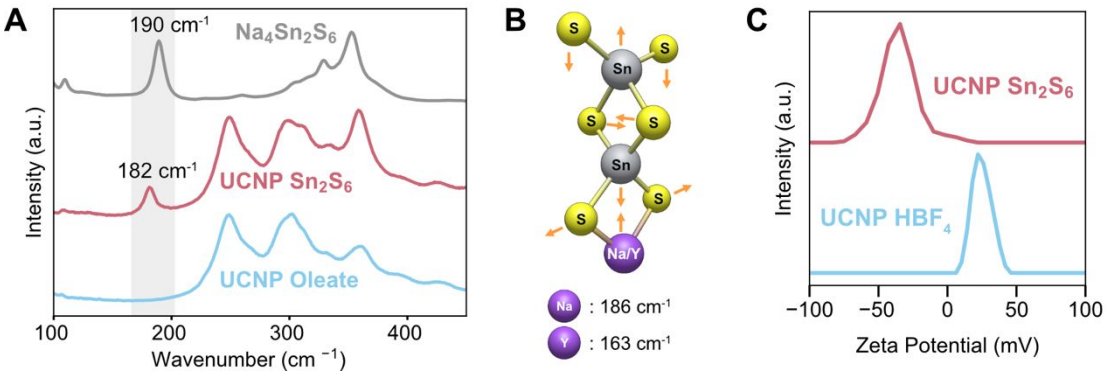

Figure 1. (A) Raman spectra of $Na_4Sn_2S_6$ and 14-nm $NaYF_4$: 30% Yb^{3+}, 0.5% Tm^{3+} UCNPs capped with oleate or $Sn_2S_6^{4-}$ ligands. (B) The relevant Raman-active vibrational mode of $(NaSn_2S_6)^{3-}$ and $(YSn_2S_6)^{3-}$ compounds and their vibrational energies. (C) Zeta potential of 15-nm $NaYF_4$: 20% Yb^{3+}, 2% Er^{3+} UCNPs after ligand stripping and after Sn_2S_6 binding.

To better understand the molecular origin of our Raman spectra, we carried out density functional theory (DFT) calculations. Since $Sn_2S_6^{4-}$ and $NaYF_4$ have overlapping peaks in the 200–450 cm^{-1} region, we focused our analysis on the 180–190 cm^{-1} peak. Our DFT calculations show that this vibrational mode can be attributed to a bending mode that involves the vibration of all bonds within $Sn_2S_6^{4-}$ as well as its bonds to the metal ion. (**Figure 1B**). The calculation also revealed that $Sn_2S_6^{4-}$ bound to a Na^+ ion has a higher frequency Raman mode (186 cm^{-1}) compared to $Sn_2S_6^{4-}$ bound to a Y^+ ion (163 cm^{-1}). Thus, the DFT results support that our experimental redshift in the Raman peak is consistent with the binding of $Sn_2S_6^{4-}$ to the UCNP surface.

Successful $Sn_2S_6^{4-}$ ligand exchange was also supported by zeta potential measurements that show a charge inversion from +30 mV after HBF_4 stripping to −40 mV upon $Sn_2S_6^{4-}$ functionalization (**Figure 1C**). Dynamic light scattering measurements showed an increase in the mean hydrodynamic radius from 16 nm to 68 nm, indicating some minor aggregation upon ligand exchange (**Figure S1**).

We then used electron microscopy to probe physical and compositional changes during the ligand exchange process (**Figure 2A–B**). After carrying out a direct $Sn_2S_6^{4-}$ exchange, we observe a decrease of about 2 nm in the average center-to-center distance of the UCNPs, confirming that the bulkier oleate has been replaced by more compact $Sn_2S_6^{4-}$. EDS elemental mapping showed that sulfur and tin were uniformly dispersed among the UNCPs at both the nanoscale (**Figure 2C** and **S2**) and microscale (**Figure S3**). We also used the elemental mapping to estimate the $Sn_2S_6^{4-}$ ligand coverage at 0.7 ligands/nm^2 (see discussion and Figure S7 in the Supplementary Information for details).

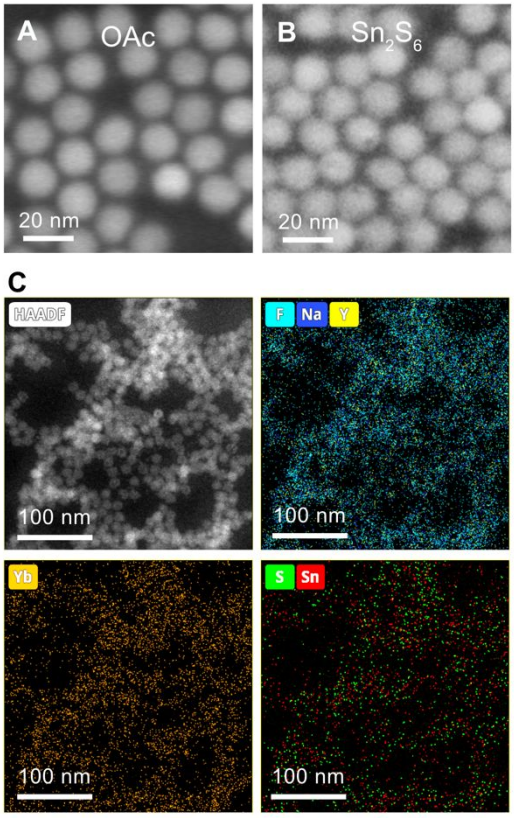

Figure 2. Nanoscale characterization of 14-nm $NaYF_4$: 30% Yb^{3+}, 0.5% Tm^{3+} UCNPs capped with $Sn_2S_6^{4-}$ ligands. (A−B) Scanning transmission electron microscope images (STEM) of UCNPs capped with (A) oleate ligands or (B) $Sn_2S_6^{4-}$ ligands via direct ligand exchange. The center-to-center distances are 18.3 ± 0.9 nm (oleate-capped) and 16.0 ± 1.1 nm ($Sn_2S_6^{4-}$-capped). (C) High-angle annular dark-field imaging (HAADF) STEM and EDS elemental maps of Sn_2S_6-capped UCNPs obtained via indirect ligand exchange.

In summary, all analyses validate that $NaYF_4$ UCNPs can be effectively functionalized with $Sn_2S_6^{4-}$ ligands through either direct or indirect ligand exchange approaches. However, the indirect exchange gives a significantly higher yield and hence was our preferred method for subsequent experiments.

Enhancement of upconversion luminescence by $Sn_2S_6^{4-}$ ligands

We hypothesized that functionalizing UCNPs with low-vibrational-energy $Sn_2S_6^{4-}$ would increase their UCL by reducing non-radiative relaxation pathways. To quantitatively assess the effect of $Sn_2S_6^{4-}$ ligands on the UCL, we measured the UCL from the same solution of ligand-stripped UCNPs before and after titrating them with $Sn_2S_6^{4-}$ ligands, with overnight equilibration used to ensure complete exchange. We compared $Sn_2S_6^{4-}$-capped UCNPs with stripped UNCPs

(rather than with oleate-capped ligands) as this ensures consistency in the UCNP concentration and type of solvent (NMF).

Upon functionalizing 8-nm-diameter $NaYF_4$: 20% Gd^{3+}, 49% Yb^{3+}, 1% Tm^{3+} UCNPs with $Sn_2S_6^{4-}$ ligands, we observed 5- to 16-fold enhancements in the UCL intensities of different radiative transitions of Tm^{3+}, compared to ligand-stripped UCNPs capped with BF_4^- (**Figure 3A–B**). In general, we find that higher energy (shorter wavelength) transitions have stronger enhancements, a trend consistent with previous studies using organic ligands.[20] One exception is the 450 nm emission, which has the lowest enhancement; we attribute this deviation from the trend to a small but non-negligible absorption from the $Sn_2S_6^{4-}$ ligands. We also observe increases in the UCL of 15-nm $NaYF_4$: 40% Yb^{3+}, 60% Er^{3+}, with enhancement factors of 9–10 for the green and red emission lines (**Figure 3C–D**). Kinetic time series measurements show that the enhancement factor rapidly increases within the first 4 minutes after $Sn_2S_6^{4-}$ coordination and reaches saturation in about 80 minutes (**Figure S4**).

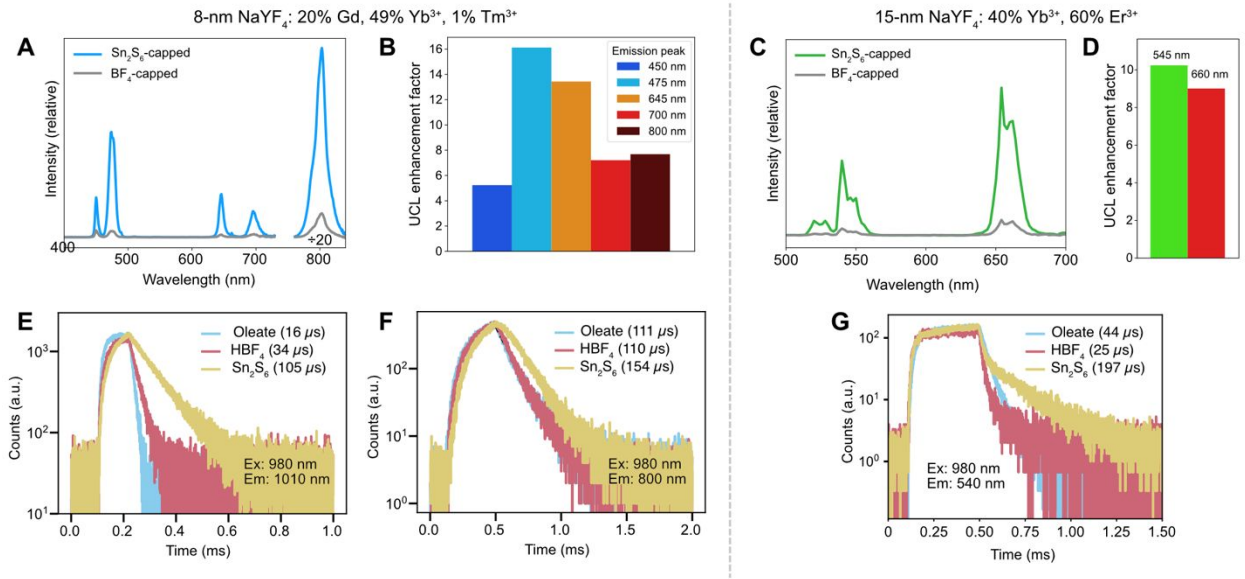

Figure 3. Upconversion luminescence (UCL) of $Sn_2S_6^{4-}$-capped UCNPs. (A–D) UCL spectra and enhancement factors of Yb^{3+}/Tm^{3+}-doped (A–B) and Yb^{3+}/Er^{3+}-doped (C–D) UCNPs before and after adding Sn_2S_6 ligands. (E–F) Fluorescence lifetimes of the 1010 nm (E) or 800 nm (F) emissions from 8-nm $NaYF_4$: 20% Gd^{3+}, 49% Yb^{3+}, 1% Tm^{3+} UCNPs with different surface treatments using 980 nm excitation. (G) Fluorescence lifetimes of the 540 nm emission 6-nm $NaYF_4$: 20% Gd^{3+}, 20% Yb^{3+}, 2% Er^{3+} UCNPs with different surface treatments using 980 nm excitation.

The UCL enhancement due to the reduction in vibrational relaxation is corroborated by the lengthening of luminescence decay lifetimes upon $Sn_2S_6^{4-}$ exchange. When directly excited with

980 nm pulses, Yb^{3+}/Tm^{3+}-doped UCNPs (**Figure 3E–F**) exhibited a significant increase in the lifetime of the Yb^{3+} 1010 nm emission, from 34 μs to 105 μs, which is also longer than the emission lifetime of oleate-capped UCNPs (16 μs). A significant but smaller increase in the lifetime is also observed for the Tm^{3+} 800 nm emission (980 nm excitation) upon $Sn_2S_6^{4-}$ exchange (154 μs) compared with that of ligand-stripped UCNPs (110 μs) and oleate-capped UCNPs (111 μs). This increase in lifetime is also observed for the 540 nm emission from $Sn_2S_6^{4-}$-capped Yb^{3+}/Er^{3+} UCNPs (**Figure 3G**), which had an intensity-weighted lifetime of 197 μs, compared to a lifetime of 25 μs for ligand-stripped UCNPs and 44 μs for oleate-capped UCNPs (see Supplementary Information for details on lifetime measurements and averaging). We note that nearly all the UCNP decay curves shown in our work (and other work) exhibit multiple decay components. Our prior work has demonstrated that UCNP lifetimes are complicated to interpret due the complex energy transfer networks among dopants;[26] hence, it is difficult to conclusively attribute specific components in a decay curve to a specific process.

To elucidate the mechanism behind this UCL enhancement, we measured the enhancement factors for UCNPs with different physical and chemical parameters. We investigated how the ligand enhancement is affected by the presence of an inert shell. For 14-nm $NaYF_4$: 30%Yb^{3+}, 0.5% Tm^{3+} cores, we measured enhancement factors of 3-5 upon ligand functionalization. Upon the growth of a 5-nm shell, the UCL of the UCNPs is significantly enhanced compared to the UCNP cores, an effect that is well established. However, subsequent functionalization of the core-shell UCNPs by $Sn_2S_6^{4-}$ ligands does not result in further UCL enhancement (**Figure 4A**). This implies that the $Sn_2S_6^{4-}$ enhancement only occurs when ligands are in relatively close proximity to the photo-active dopant ions. We thus conclude that $Sn_2S_6^{4-}$ molecules enhance UCL by reducing the available ligand vibrational modes that are coupled to excited dopant ions (**Scheme 2**).

Additionally, we found much smaller UCL enhancements for larger 52-nm UCNPs compared to smaller 15-nm UCNPs (**Figure 4B**). The reduced enhancement is likely due to the smaller surface-to-volume ratios of larger UCNPs, which are well known to be less susceptible to surface quenching.[27] We also found that UCNPs with higher doping concentrations (40% Yb^{3+}, 60% Er^{3+}) had higher enhancement factors (9–10), while UCNPs with lower doping concentrations (20% Yb^{3+}, 2% Er^{3+}, with similar sizes) have smaller enhancement factors (~2) (**Figure 4C**).

Finally, we found comparable enhancements for both cubic- and hexagonal-phase UCNPs (**Figure 4D**), revealing a negligible effect of the crystal structure on UCL enhancement.

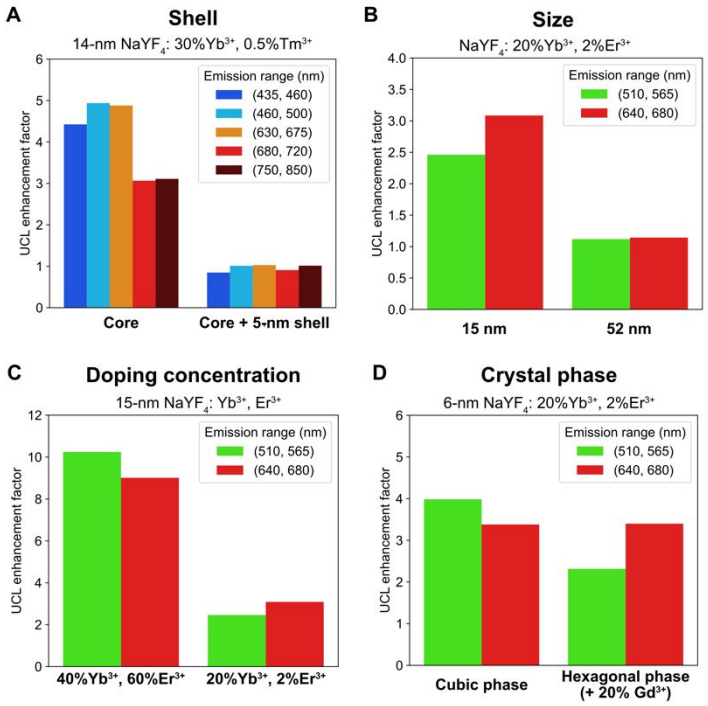

Figure 4. Effect of UCNP parameters on the UCL enhancements by $Sn_2S_6^{4-}$ ligands. Changes in the UCL enhancement factors upon growing an inert shell (A), or upon changing the doping concentration (B), size (C), or crystal phase (D). In all cases, the concentration of the $Na_4Sn_2S_6$ ligands was kept constant at 0.5 mM.

Scheme 2. Proposed mechanism of UCL enhancement by $Sn_2S_6^{4-}$ ligands.

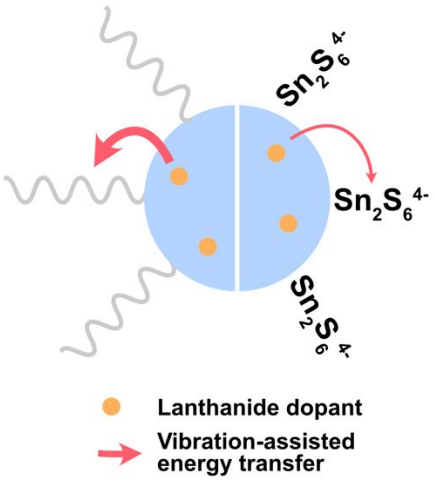

Fabrication of a UCNP-SnS_2 nanocomposite

$Sn_2S_6^{4-}$ complexes have been previously shown to transform into a semiconducting SnS_2 matrix upon annealing at relatively modest temperatures (<200 °C).[28] This property has led to the exploration of $Sn_2S_6^{4-}$ as a promising ligand for integrating colloidal nanomaterials in electronic or optoelectronic devices. For instance, annealing $Sn_2S_6^{4-}$-capped QDs resulted in a QD-SnS_2 composite that had high charge carrier mobilities and could be used as the active component in transistors.[21] Here, we explore the fabrication of a UCNP-SnS_2 nanocomposite and evaluate its potential as an upconversion-based photodetector.

Annealing of the $Na_4Sn_2S_6$ ligand without UCNPs resulted in a film with a characteristic SnS_2 Raman peak at 314 cm^{-1} (**Figure 5A**, green line). Upon annealing the $Sn_2S_6^{4-}$-capped UCNPs at 350 °C to form the UCNP-SnS_2 composite, we observed the disappearance of the 182 cm^{-1} peak and the weakening of the 360 cm^{-1} peak, consistent with the decomposition of $Sn_2S_6^{4-}$ (**Figure 5A**, blue line). The identification of the SnS_2 peak for the UCNP-SnS_2 is more challenging due to interfering $NaYF_4$ peaks.

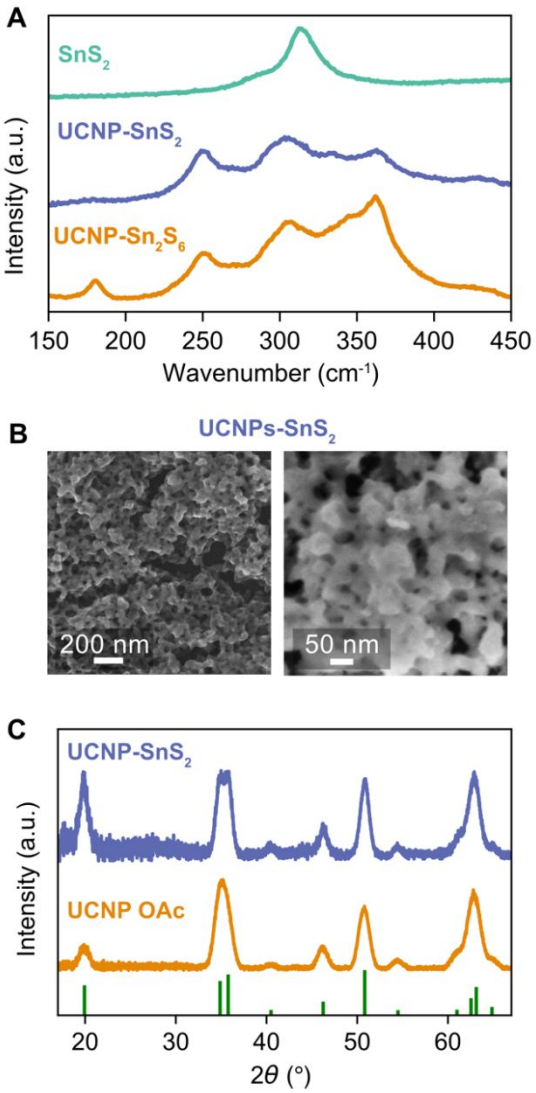

Figure 5. Annealing $Sn_2S_6^{4-}$-capped 9-nm $NaYF_4$: 8% Tm^{3+} UCNPs at 350 °C to form a UCNP-SnS_2 nanocomposite. (A) Raman spectra of the $Sn_2S_6^{4-}$-capped UCNPs before (orange line) and after (blue line) annealing. Also shown is the spectrum of the SnS_2 matrix formed by annealing $Na_4Sn_2S_6$ (green line). (B) SEM images of the UCNPs embedded in the SnS_2 matrix. (C) X-ray diffraction spectra of the UCNPs-SnS_2 nanocomposite (blue line) and oleate-capped UCNPs (orange line).

Scanning electron microscopy further supports the formation of a UCNP-SnS_2 composite. The composite with 9-nm UCNPs (**Figure 5B**) exhibits interconnected nanoscale nodules, significantly different than the original $Sn_2S_6^{4-}$-capped UCNPs, which were clearly separated (**Figure 2B**). These nodules are attributed to the formation of a SnS_2 matrix made from the decomposition and fusing of the $Sn_2S_6^{4-}$ ligands. An alternative hypothesis is that these nodules are from the sintering and grain growth of the $NaYF_4$ UCNPs themselves. However, this hypothesis can be rejected since powder X-ray diffraction peaks do not significantly narrow

following annealing (**Figure 5C**), indicate no significant increase in the size of the $NaYF_4$ domains. Additional characterization (e.g., X-ray photoelectron spectroscopy) could potentially be used to further confirm the formation of the $NaYF_4/SnS_2$ composite.

Our analyses thus support the formation of nanoscale upconverting emitters embedded in a semiconducting matrix. This composite allows the desirable optical properties of UCNPs to be retained while adding the important capability to electronically interface with each UCNP through the semiconducting matrix. Further work could include more detailed studies on how the annealing and formation of the UCNP-SnS_2 composites affect UCL properties (e.g., intensity, linewidth, peak positions).

UV and NIR photoconductivity of the UCNP-SnS_2 nanocomposite

One benefit of encapsulating UCNPs in a continuous semiconductor matrix is that it allows for easier integration of UCNP into electronic devices. While the dielectric UCNPs and their ligands are insulating, UCNP/semiconductor composites could in principle provide a pathway to new solution-processable optoelectronic devices that incorporate UCNPs.

To demonstrate the capabilities of the UCNP-SnS_2 nanocomposite, we evaluated its use as a photodetector (**Figure 6A**). To fabricate a simple proof-of-concept device, we drop-cast $Sn_2S_6^{4-}$-capped UCNPs onto interdigitated ITO electrodes on glass that was obtained commercially (**Figure 6B**) and annealed the sample at 350 °C to form the UCNP-SnS_2 composite. We hypothesized that the embedded UCNPs would absorb IR light and emit upconverted UV and blue light that could be absorbed by the surrounding SnS_2 matrix (**Scheme 3**). The resulting increase in the concentration of charge carriers in the SnS_2 semiconductor in principle should lead to an increase in the observed current at a constant applied voltage.

As a first step, we confirmed that our photoconductor can detect UV light that is absorbed directly by the SnS_2 matrix. Indeed, we observed a clear increase in the current when 395 nm light (~60 mW/cm^2) was incident on the substrate (**Figure 6C**). Next, we substituted the 395 nm light for a 980 nm laser light source (~300 mW/cm^2) and successfully detected an increase in current upon irradiation (**Figure 6D**). Since ITO and SnS_2 have negligible absorption at 980 nm, the photocurrent is attributed to absorption by the UCNP followed by upconversion and transfer of energy to the SnS_2 matrix. While the photocurrent was weaker than that induced by 395 nm light, the response can be improved by increasing the film thickness and quality, optimizing the UCNP

loading percent, and engineering a better overlap between the emission of the UCNP and absorption of the semiconducting matrix. This proof-of-concept device demonstrates a viable path for using semiconducting ligands and matrices to electronically interface with UCNPs within an optoelectronic device, circumventing the physical and processing challenges associated with simply mixing UCNPs with SnS_2 powder.

For all our devices, we also consistently observed a decrease in the background current as a function of time after application of the voltage. When the voltage was stopped and restarted, the current level was reset to its original value. This implies that this decrease in current is due to capacitance, which we attribute to misalignment between the energy levels of ITO and our active materials. Further optimization of the contact material should reduce or remove this effect.

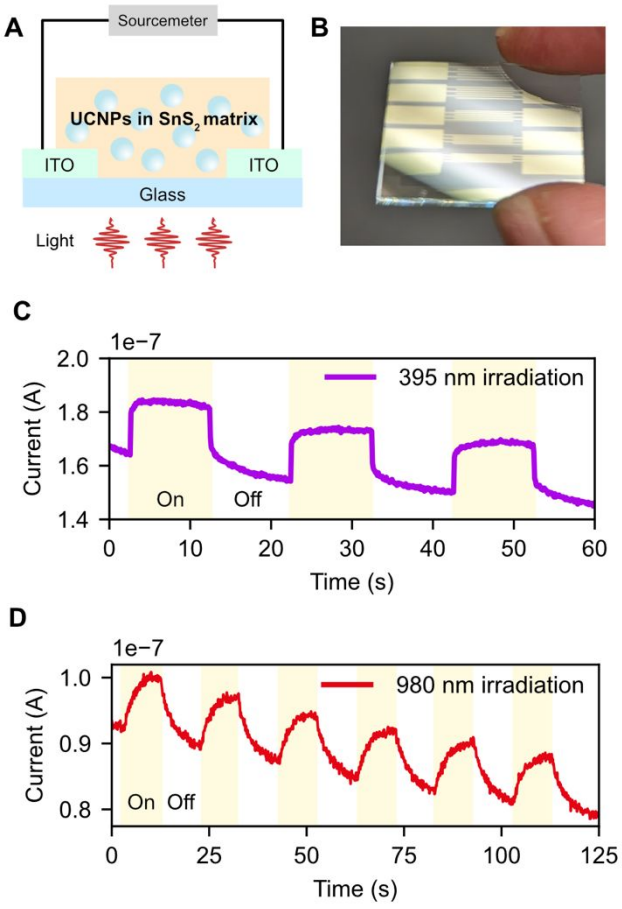

Figure 6. Photoconductivity of a UCNPs-SnS_2 nanocomposite film. (A) Device schematic of the photoconductor. (B) Picture of the interdigitated indium tin oxide (ITO) electrodes. (C−D) Photoconductivity time curves of a film of 24-nm $NaYF_4$: 30% Yb^{3+}, 0.5% Tm^{3+}/$NaYF_4$ UCNPs (14 nm core/5 nm shell) in a SnS_2 matrix upon 395 nm (C) or 980 nm (D) irradiation.

Scheme 3. Proposed mechanism of photodetection by the UCNP-SnS_2 nanocomposite.

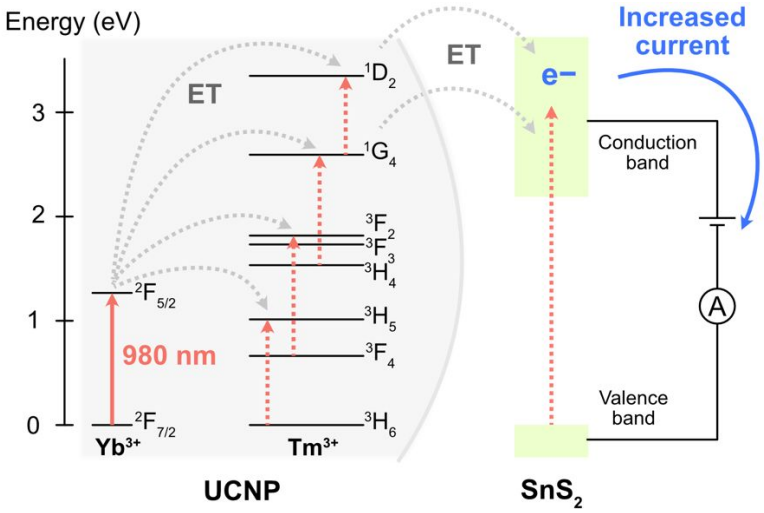

Conclusions

In this study, we investigated the surface functionalization of lanthanide-doped UCNPs with $Sn_2S_6^{4-}$ inorganic metal complexes and verified the ligand exchange via Raman spectroscopy and EDS elemental mapping. We found that the $Sn_2S_6^{4-}$ ligands can enhance the UCL intensity of both Yb^{3+}/Tm^{3+}- and Yb^{3+}/Er^{3+}-doped UCNPs, with enhancement factors up to 16 for small, highly doped UCNPs. Upon annealing, these $Sn_2S_6^{4-}$-capped UCNPs can also be transformed into a nanocomposite of UCNPs embedded within a matrix of semiconducting SnS_2. This nanocomposite can be used to harness the nonlinear optical properties of UCNPs in charge-based devices such as photodetectors. To demonstrate this, we tested a proof-of-concept UCNP-SnS_2 device that displays photoconductive behavior under both UV and NIR light. We have also demonstrated in preliminary work that $Sn_2S_6^{4-}$-functionalization can be extended to photon avalanching nanoparticles with no significant changes to their nonlinear responses (see Supplementary Information and Figure S5 for details).[6,29,30]

Our findings show how semiconducting inorganic complexes with low vibrational energies can be used to enhance the optical properties of UCNPs while seamlessly facilitating the fabrication of a low-phonon-energy matrix that allows UCNPs to be accessed electronically. With further optimization, this approach should be extensible to other UCNP host materials and other nanoscale emitters that can benefit from a non-epitaxial, low-vibrational-energy environment.

Methods

$Na_4Sn_2S_6$•$14H_2O$ synthesis

The synthesis of $Na_4Sn_2S_6$•$14H_2O$ was carried out according to previous reports.[24,31] To a 100 mL glass bottle, Na_2S•$9H_2O$ (14.4 g, 60 mmol) and 90 mL DI H_2O were added and stirred for 5 hr to form a clear solution. To a 50 mL centrifuge tube, $SnCl_4$•$5H_2O$ (7.0 g, 20 mmol) and 5 mL DI H_2O were added and stirred for 5 hr to form a clear solution. The $SnCl_4$ solution was then added dropwise (using a separatory funnel) into the Na_2S solution while stirring. The resulting crude $Na_4Sn_2S_6$ solution was then stirred overnight. The crude solution was then added dropwise to 300 mL acetone in a 500 mL glass bottle under vigorous stirring. A yellowish-white precipitate is formed during this process. After the addition, the suspension is placed in the freezer for 5 hr. At the same time, 100 mL of neat acetone in a separate glass bottle is also chilled in the freezer for 5 hr. At this point, the chilled suspension is decanted and the solid is shaken together with 100 mL of chilled acetone. The suspension is decanted again and the solid is dried in a vacuum oven at room temperature overnight to give an off-white pale precipitate (5.53 g, 72% yield).

$Na_4Sn_2S_6$ ligand exchange of oleate-capped $NaYF_4$ UCNPs.

Exchange with intermediate ligand stripping. To 100 uL of UCNPs (~100 mg/mL), was added 1 mL of toluene. Then, 25 uL of 0.5 M HBF_4 in DMF was added to the solution, which immediately resulted in the formation of a precipitate. [To make a 0.5 M HBF_4 stock solution, HBF_4-diethyl ether solution (343 uL, 2.5 mmol) was slowly added to DMF (4.66 mL). *Caution*: exothermic reaction.] The suspension was sonicated for 5 mins followed by centrifugation (5000 rpm, 2021*g*, 1 min). The UCNPs were then washed twice with 0.3 mL DMF/0.7 mL toluene and redispersed in 2 mL of DMF. To this solution was added 50 mM $Na_4Sn_2S_6$ solution in NMF (20 – 200 uL) to achieve a $Na_4Sn_2S_6$ ligand concentration of 0.5 – 5 mmol. The solution was left to sit overnight, centrifuged (5000 rpm, 2021*g*, 1 min), and redispersed in DMF with sonication.

Direct exchange (low yield). To 200 uL of UCNPs (~100 mg/mL), was added 1 mL of ethanol followed by centrifugation (3000 rpm, 728*g*, 30 s). NMF (1 mL) was added followed by vortexing to get a suspension. To the suspension, 20 uL of 50 mM $Na_4Sn_2S_6$ solution in NMF was added followed by vortexing and then sonication for 1 hr. The suspension was centrifuged (5000

rpm, 2021*g*, 30 s) to remove unreacted UCNPs. To the supernatant, acetonitrile (2 mL) was added followed by centrifugation (10,000 rpm, 8084*g*, 1 min). The residue was redissolved in 100 uL NMF, to which was added 400 uL acetonitrile. The suspension was centrifuged (10,000 rpm, 8084*g*, 1 min) and finally redissolved in 100 uL NMF.

Formation of UCNP-SnS_2 composite by annealing $Sn_2S_6^{4-}$-capped UCNPs. $Sn_2S_6^{4-}$-capped UCNPs were deposited on a Si wafer or glass slide followed by annealing on a hot plate at 350 °C for about 15 min.

Conflicts of interest

There are no conflicts of interest to declare.

Acknowledgments

This work was supported by the U.S. Department of Energy (DOE), Office of Science, Office of Basic Energy Sciences, Chemical Sciences, Geosciences, and Biosciences Division, Separations Program, at the Lawrence Berkeley National Laboratory under Contract No. DE-AC02-05CH11231. Work at the Molecular Foundry was supported by the Office of Science, Office of Basic Energy Sciences, of the U.S. Department of Energy under Contract No. DE-AC02-05CH11231.

References

(1) Haase, M.; Schäfer, H. Upconverting Nanoparticles. *Angew. Chem. Int. Ed.* **2011**, *50* (26), 5808–5829. https://doi.org/10.1002/anie.201005159.
(2) Xia, X.; Sivonxay, E.; Helms, B. A.; Blau, S. M.; Chan, E. M. Accelerating the Design of Multishell Upconverting Nanoparticles through Bayesian Optimization. *Nano Lett.* **2023**, *23* (23), 11129–11136. https://doi.org/10.1021/acs.nanolett.3c03568.
(3) Qi, X.; Lee, C.; Ursprung, B.; Skripka, A.; Schuck, P. J.; Chan, E. M.; Cohen, B. E. Short-Wave Infrared Upconverting Nanoparticles. *J. Am. Chem. Soc.* **2024**, *146* (43), 29292–29296. https://doi.org/10.1021/jacs.4c11181.
(4) Mettenbrink, E. M.; Yang, W.; Wilhelm, S. Bioimaging with Upconversion Nanoparticles. *Adv. Photonics Res.* **2022**, *3* (12), 2200098. https://doi.org/10.1002/adpr.202200098.

(5) Ye, Z.; Harrington, B.; Pickel, A. D. Optical Super-Resolution Nanothermometry via Stimulated Emission Depletion Imaging of Upconverting Nanoparticles. *Sci. Adv.* **2024**, *10* (29), eado6268. https://doi.org/10.1126/sciadv.ado6268.
(6) Lee, C.; Xu, E. Z.; Liu, Y.; Teitelboim, A.; Yao, K.; Fernandez-Bravo, A.; Kotulska, A. M.; Nam, S. H.; Suh, Y. D.; Bednarkiewicz, A.; Cohen, B. E.; Chan, E. M.; Schuck, P. J. Giant Nonlinear Optical Responses from Photon-Avalanching Nanoparticles. *Nature* **2021**, *589* (7841), 230–235. https://doi.org/10.1038/s41586-020-03092-9.
(7) Lee, C.; Xu, E. Z.; Kwock, K. W. C.; Teitelboim, A.; Liu, Y.; Park, H. S.; Ursprung, B.; Ziffer, M. E.; Karube, Y.; Fardian-Melamed, N.; Pedroso, C. C. S.; Kim, J.; Pritzl, S. D.; Nam, S. H.; Lohmueller, T.; Owen, J. S.; Ercius, P.; Suh, Y. D.; Cohen, B. E.; Chan, E. M.; Schuck, P. J. Indefinite and Bidirectional Near-Infrared Nanocrystal Photoswitching. *Nature* **2023**, *618* (7967), 951–958. https://doi.org/10.1038/s41586-023-06076-7.
(8) Pan, J.-A.; Skripka, A.; Lee, C.; Qi, X.; Pham, A. L.; Woods, J. J.; Abergel, R. J.; Schuck, P. J.; Cohen, B. E.; Chan, E. M. Ligand-Assisted Direct Lithography of Upconverting and Avalanching Nanoparticles for Nonlinear Photonics. *J. Am. Chem. Soc.* **2024**, *146* (11), 7487–7497. https://doi.org/10.1021/jacs.3c12850.
(9) Skripka, A.; Zhang, Z.; Qi, X.; Ursprung, B.; Ercius, P.; Cohen, B. E.; Schuck, P. J.; Jaque, D.; Chan, E. M. Intrinsic Optical Bistability of Photon Avalanching Nanocrystals. November 21, 2024. https://doi.org/10.1038/s41566-024-01577-x.
(10) Bednarkiewicz, A.; Szalkowski, M.; Majak, M.; Korczak, Z.; Misiak, M.; Maćkowski, S. All-Optical Data Processing with Photon-Avalanching Nanocrystalline Photonic Synapse. *Adv. Mater.* **2023**, *35* (42), 2304390. https://doi.org/10.1002/adma.202304390.
(11) Li, J.; Shen, Y.; Liu, Y.; Shi, F.; Ren, X.; Niu, T.; Zhao, K.; Liu, S. F. Stable High-Performance Flexible Photodetector Based on Upconversion Nanoparticles/Perovskite Microarrays Composite. *ACS Appl. Mater. Interfaces* **2017**, *9* (22), 19176–19183. https://doi.org/10.1021/acsami.7b03229.
(12) Heer, S.; Kömpe, K.; Güdel, H.-U.; Haase, M. Highly Efficient Multicolour Upconversion Emission in Transparent Colloids of Lanthanide-Doped NaYF4 Nanocrystals. *Adv. Mater.* **2004**, *16* (23–24), 2102–2105. https://doi.org/10.1002/adma.200400772.
(13) Zhang, Z.; Skripka, A.; Dahl, J. C.; Dun, C.; Urban, J. J.; Jaque, D.; Schuck, P. J.; Cohen, B. E.; Chan, E. M. Tuning Phonon Energies in Lanthanide-Doped Potassium Lead Halide Nanocrystals for Enhanced Nonlinearity and Upconversion. *Angew. Chem. Int. Ed.* **2023**, *62* (1), e202212549. https://doi.org/10.1002/anie.202212549.
(14) Homann, C.; Krukewitt, L.; Frenzel, F.; Grauel, B.; Würth, C.; Resch-Genger, U.; Haase, M. NaYF4:Yb,Er/NaYF4 Core/Shell Nanocrystals with High Upconversion Luminescence Quantum Yield. *Angew. Chem. Int. Ed.* **2018**, *57* (28), 8765–8769. https://doi.org/10.1002/anie.201803083.
(15) Geitenbeek, R. G.; Prins, P. T.; Albrecht, W.; van Blaaderen, A.; Weckhuysen, B. M.; Meijerink, A. NaYF4:Er3+,Yb3+/SiO2 Core/Shell Upconverting Nanocrystals for Luminescence Thermometry up to 900 K. *J. Phys. Chem. C* **2017**, *121* (6), 3503–3510. https://doi.org/10.1021/acs.jpcc.6b10279.
(16) Sedlmeier, A.; Gorris, H. H. Surface Modification and Characterization of Photon-Upconverting Nanoparticles for Bioanalytical Applications. *Chem. Soc. Rev.* **2015**, *44* (6), 1526–1560. https://doi.org/10.1039/C4CS00186A.
(17) Garfield, D. J.; Borys, N. J.; Hamed, S. M.; Torquato, N. A.; Tajon, C. A.; Tian, B.; Shevitski, B.; Barnard, E. S.; Suh, Y. D.; Aloni, S.; Neaton, J. B.; Chan, E. M.; Cohen, B. E.;

Schuck, P. J. Enrichment of Molecular Antenna Triplets Amplifies Upconverting Nanoparticle Emission. *Nat. Photonics* **2018**, *12* (7), 402–407. https://doi.org/10.1038/s41566-018-0156-x.

(18) Kim, M. A.; Ai, Q.; Norquist, A. J.; Schrier, J.; Chan, E. M. Active Learning of Ligands That Enhance Perovskite Nanocrystal Luminescence. *ACS Nano* **2024**, *18* (22), 14514–14522. https://doi.org/10.1021/acsnano.4c02094.

(19) Boles, M. A.; Ling, D.; Hyeon, T.; Talapin, D. V. The Surface Science of Nanocrystals. *Nat. Mater.* **2016**, *15* (2), 141–153. https://doi.org/10.1038/nmat4526.

(20) Xu, H.; Han, S.; Deng, R.; Su, Q.; Wei, Y.; Tang, Y.; Qin, X.; Liu, X. Anomalous Upconversion Amplification Induced by Surface Reconstruction in Lanthanide Sublattices. *Nat. Photonics* **2021**, *15* (10), 732–737. https://doi.org/10.1038/s41566-021-00862-3.

(21) Kovalenko, M. V.; Scheele, M.; Talapin, D. V. Colloidal Nanocrystals with Molecular Metal Chalcogenide Surface Ligands. *Science* **2009**, *324* (5933), 1417–1420. https://doi.org/10.1126/science.1170524.

(22) Jang, J.; Dolzhnikov, D. S.; Liu, W.; Nam, S.; Shim, M.; Talapin, D. V. Solution-Processed Transistors Using Colloidal Nanocrystals with Composition-Matched Molecular "Solders": Approaching Single Crystal Mobility. *Nano Lett.* **2015**, *15* (10), 6309–6317. https://doi.org/10.1021/acs.nanolett.5b01258.

(23) Ostrowski, A. D.; Chan, E. M.; Gargas, D. J.; Katz, E. M.; Han, G.; Schuck, P. J.; Milliron, D. J.; Cohen, B. E. Controlled Synthesis and Single-Particle Imaging of Bright, Sub-10 Nm Lanthanide-Doped Upconverting Nanocrystals. *ACS Nano* **2012**, *6* (3), 2686–2692. https://doi.org/10.1021/nn3000737.

(24) Oh, Y.; Bag, S.; Malliakas, C. D.; Kanatzidis, M. G. Selective Surfaces: High-Surface-Area Zinc Tin Sulfide Chalcogels. *Chem. Mater.* **2011**, *23* (9), 2447–2456. https://doi.org/10.1021/cm2003462.

(25) Wilhelm, S.; Hirsch, T.; Patterson, W. M.; Scheucher, E.; Mayr, T.; Wolfbeis, O. S. Multicolor Upconversion Nanoparticles for Protein Conjugation. *Theranostics* **2013**, *3* (4), 239–248. https://doi.org/10.7150/thno.5113.

(26) Teitelboim, A.; Tian, B.; Garfield, D. J.; Fernandez-Bravo, A.; Gotlin, A. C.; Schuck, P. J.; Cohen, B. E.; Chan, E. M. Energy Transfer Networks within Upconverting Nanoparticles Are Complex Systems with Collective, Robust, and History-Dependent Dynamics. *J. Phys. Chem. C* **2019**, *123* (4), 2678–2689. https://doi.org/10.1021/acs.jpcc.9b00161.

(27) Gargas, D. J.; Chan, E. M.; Ostrowski, A. D.; Aloni, S.; Altoe, M. V. P.; Barnard, E. S.; Sanii, B.; Urban, J. J.; Milliron, D. J.; Cohen, B. E.; Schuck, P. J. Engineering Bright Sub-10-Nm Upconverting Nanocrystals for Single-Molecule Imaging. *Nat. Nanotechnol.* **2014**, *9* (4), 300–305. https://doi.org/10.1038/nnano.2014.29.

(28) Mitzi, D. B.; Kosbar, L. L.; Murray, C. E.; Copel, M.; Afzali, A. High-Mobility Ultrathin Semiconducting Films Prepared by Spin Coating. *Nature* **2004**, *428* (6980), 299–303. https://doi.org/10.1038/nature02389.

(29) Szalkowski, M.; Kotulska, A.; Dudek, M.; Korczak, Z.; Majak, M.; Marciniak, L.; Misiak, M.; Prorok, K.; Skripka, A.; James Schuck, P.; M. Chan, E.; Bednarkiewicz, A. Advances in the Photon Avalanche Luminescence of Inorganic Lanthanide-Doped Nanomaterials. *Chem. Soc. Rev.* **2025**. https://doi.org/10.1039/D4CS00177J.

(30) Skripka, A.; Lee, M.; Qi, X.; Pan, J.-A.; Yang, H.; Lee, C.; Schuck, P. J.; Cohen, B. E.; Jaque, D.; Chan, E. M. A Generalized Approach to Photon Avalanche Upconversion in

Luminescent Nanocrystals. *Nano Lett.* **2023**, *23* (15), 7100–7106. https://doi.org/10.1021/acs.nanolett.3c01955.

(31) Jung, S. M.; Kang, H. L.; Won, J. K.; Kim, J.; Hwang, C.; Ahn, K.; Chung, I.; Ju, B.-K.; Kim, M.-G.; Park, S. K. High-Performance Quantum Dot Thin-Film Transistors with Environmentally Benign Surface Functionalization and Robust Defect Passivation. *ACS Appl. Mater. Interfaces* **2018**, *10* (4), 3739–3749. https://doi.org/10.1021/acsami.7b13997.

Data will be made available upon request by contacting the authors.